

ORIGINAL ARTICLE

Patient-derived xenograft mouse models to investigate tropism to the central nervous system and retina of primary and secondary central nervous system lymphoma

Lisa Kristina Isbell¹ | Cordula Tschuch² | Soroush Doostkam³ | Silvia Waldeck¹ |
Geoffroy Andrieux^{4,5} | Khalid Shoumariyeh^{1,5} | Dorothee Lenhard² |
Hans Eckart Schaefer⁶ | Peter Christoph Reinacher^{7,8} | Ingrid Bartsch¹ |
Milena Pantic¹ | Janaki Manoja Vinnakota¹ | Vinodh Kakkassery⁹ |
Elisabeth Schorb¹ | Florian Scherer^{1,5} | Anna Verena Frey⁶ | Melanie Boerries^{4,5} |
Gerald Illerhaus¹⁰ | Justus Duyster^{1,5} | Julia Schueler² | Nikolas von Bubnoff^{1,5,11}

¹Department of Medicine I, Medical Center, University of Freiburg, Faculty of Medicine, Freiburg, Germany

²Charles River Discovery Research Services GmbH, Freiburg, Germany

³Institute of Neuropathology, Medical Center, University of Freiburg, Faculty of Medicine, Freiburg, Germany

⁴Institute of Medical Bioinformatics and Systems Medicine (IBSM), Medical Center, University of Freiburg, Faculty of Medicine, Freiburg, Germany

⁵German Cancer Consortium (DKTK), partner site Freiburg, Germany and German Cancer Research Center (DKFZ), Heidelberg, Germany

⁶Department of Pathology, University of Freiburg, Freiburg, Germany

⁷Department of Stereotactic and Functional Neurosurgery, Medical Faculty, University of Freiburg, Freiburg, Germany

⁸Fraunhofer Institute for Laser Technology (ILT), Aachen, Germany

⁹Department of Ophthalmology, University of Luebeck, Luebeck, Germany

¹⁰Clinic of Hematology, Oncology and Palliative Care, Klinikum Stuttgart, Stuttgart, Germany

¹¹Department of Hematology and Oncology, University Hospital Schleswig-Holstein, Luebeck, Germany

Correspondence

Prof. Dr Nikolas von Bubnoff, Department of Hematology and Oncology, University Hospital Schleswig-Holstein, Ratzeburger Allee 160, 23538 Luebeck, Germany.
Email: nikolas.vonbubnoff@uksh.de

Funding information

Else Kröner-Fresenius-Stiftung; Fraunhofer foundation Germany; Deutsche Forschungsgemeinschaft; German Federal Ministry of Education and Research

Abstract

Aims: How and why lymphoma cells home to the central nervous system and vitreoretinal compartment in primary diffuse large B-cell lymphoma of the central nervous system remain unknown. Our aim was to create an in vivo model to study lymphoma cell tropism to the central nervous system.

Methods: We established a patient-derived central nervous system lymphoma xenograft mouse model and characterised xenografts derived from four primary and four secondary central nervous system lymphoma patients using immunohistochemistry, flow cytometry and nucleic acid sequencing technology. In reimplantation experiments, we analysed dissemination patterns of orthotopic and heterotopic xenografts and performed RNA sequencing of different involved organs to detect differences at the transcriptome level.

Results: We found that xenografted primary central nervous system lymphoma cells home to the central nervous system and eye after intrasplenic transplantation, mimicking central nervous system and primary vitreoretinal lymphoma pathology, respectively.

This is an open access article under the terms of the [Creative Commons Attribution-NonCommercial](https://creativecommons.org/licenses/by-nc/4.0/) License, which permits use, distribution and reproduction in any medium, provided the original work is properly cited and is not used for commercial purposes.

© 2023 The Authors. *Neuropathology and Applied Neurobiology* published by John Wiley & Sons Ltd on behalf of British Neuropathological Society.

Transcriptomic analysis revealed distinct signatures for lymphoma cells in the brain in comparison to the spleen as well as a small overlap of commonly regulated genes in both primary and secondary central nervous system lymphoma.

Conclusion: This in vivo tumour model preserves key features of primary and secondary central nervous system lymphoma and can be used to explore critical pathways for the central nervous system and retinal tropism with the goal to find new targets for novel therapeutic approaches.

KEYWORDS

CNS tropism, patient-derived xenograft, primary and secondary central nervous system lymphoma, primary vitreoretinal lymphoma

INTRODUCTION

Selective growth in the central nervous system (CNS) compartment is the key feature of primary diffuse large B-cell lymphoma (DLBCL) of the central nervous system (PCNSL) [1].

Lymphoma manifestation in the vitreoretinal compartment occurs in around 15%–20% of PCNSL cases [2, 3]. Despite the improvement of therapeutic strategies, that is, by incorporating CD20-directed treatment and high-dose chemotherapy and autologous stem cell transplantation (HCT-ASCT), the outcome remains poor compared with patients with nodal DLBCL [4–7]. Mechanisms that commit lymphoma cells to the CNS and vitreoretinal compartment are poorly understood, and it remains unclear where the transformation into a neoplastic cell takes place. Two mechanisms are commonly discussed: (1) B-cells are first recruited to the CNS through immune responses and then undergo malignant transformation or (2) malignant B-cells exterior to the CNS home selectively to the CNS compartment due to a highly selective tropism. The latter theory is supported by the detection of identical mutations in the peripheral blood mononuclear cell fraction and in lymphoma cells in the CNS [8, 9]. In 2%–10% of cases, systemic DLBCL will disseminate to the CNS, then called secondary CNS lymphoma (SCNSL) [10, 11]. SCNSL occurs as synchronous or more often metachronous CNS involvement at relapse and is associated with a poor median OS of 3.5–7 months [12].

Recently, multiomic data analysis of large DLBCL cohorts identified distinct molecular clusters correlating with different survival outcomes. PCNSL frequently harbour mutations in *MYD88* (*MYD88*^{L265P}), *CD79B* and *CARD11* as well as copy number alterations such as 9p21.3/*CDKN2A* copy loss, placing them among the newly identified “MCD” or “Cluster 5 (C5)” or “MYD88-like” DLBCL subtypes [13–20]. Despite the consensus that systemic DLBCL and SCNSL share key features with PCNSL (e.g., DLBCL histologic phenotype and CNS tropism), it is accepted that they differ on a genetic level. Although the above-mentioned studies elucidate the comprehensive genetic landscape of DLBCLs, focusing on their heterogeneity, the functional contribution of the identified genetic drivers to CNS infiltration is largely unknown. Likewise, several small studies have focused on the genetic characterisation of PCNSL [8, 21–25] as well as chemokine expression [26–28], but the relationship of the diverse findings to the selective CNS tropism remains elusive.

Key points

- The establishment and characterisation of a patient-derived xenograft mouse model of primary (PCNSL) and secondary central nervous system lymphoma (SCNSL).
- Heterotopic intrasplenic transplantation of PCNSL and SCNSL, but not systemic DLBCL without primary or secondary CNS manifestation led to homing of lymphoma cells to the central nervous system and vitreoretinal compartment, thus mimicking the central nervous system and primary vitreoretinal lymphoma pathology.
- Transcriptomic analysis of different organs affected by lymphoma identified distinct transcriptomic signatures.

In our study, we established a novel patient CNS biopsy-derived xenograft mouse model (PDX), and exploited intrasplenic adoptive transfer to study PCNSL and SCNSL spreading to the CNS and vitreoretinal compartment. Compared with reported orthotopic PDX models [29, 30], this xenograft model is to our knowledge the first to show CNS dissemination and retinal infiltration after heterotopic implantation and thus accurately mirrors CNS homing of primary CNS and vitreoretinal lymphoma (PVRL). In addition, this heterotopic PDX model allows the comparison of molecular and genetic profiles between CNS and extra-CNS lymphoma manifestations of both PCNSL and SCNSL xenografts by flow cytometry and RNAseq to identify gene expression signatures and related pathways potentially involved in CNS tropism.

PATIENTS AND METHODS

Patient material

After written informed consent, tumour tissue from diagnostic stereotactic CNS biopsies or cerebrospinal fluid (CSF) from patients with

suspicion of PCNSL, patients with systemic DLBCL with suspicion of CNS relapse, or tumour material from lymph node or bone marrow biopsies from patients with systemic DLBCL without CNS manifestations was implanted into recipient mice within 1 h. The trial protocol was approved by the local ethics committee (Albert Ludwig University Freiburg, permit number 91/14_170606).

Clinical characteristics as well as treatment and outcome parameters were collected for 24 patients (11 PCNSL, eight SCNSL and five systemic DLBCL) (Table S1, Figure S1). Table 1 shows clinical data for the patients with established PDX. All four PCNSL patients were treated within a clinical trial comprising HCT-ASCT and were in complete remission at the last follow-up. The four SCNSL patients presented with a high Ann-Arbor stage and high (CNS) – international prognostic index (IPI). Thus, three of these four patients received high-dose methotrexate in addition to R-CHOP chemotherapy, and one patient received consolidating HCT-ASCT. Despite incorporating CNS active agents in first-line treatment, all four patients subsequently developed CNS relapse and died. From two patients with systemic DLBCL without a history of CNS involvement, one patient developed a relapse 4 months after completion of first-line therapy with R-CHOP and then had a chemotherapy-refractory disease course over 2 years and died. The other patient received three courses of R-CHOP and achieved complete remission but then stopped treatment because of toxicity (Table 1, Figure S1).

Establishment of PDX models

This study was carried out in strict accordance with the recommendations in the Guide for the Care and Use of Laboratory Animals of the Society of Laboratory Animals (GV SOLAS) in an AAALAC-accredited animal facility. All animal experiments were approved by the Committee on the Ethics of Animal Experiments of the regional council (Permit Numbers: G-18/78 and G17/138).

Tumour tissue was implanted subcutaneously (s.c.) as tumour fragments, or intrasplenically (i.s.), intratibial (i.t.), or intracerebrally (i.c.) via the foramen postglenoidale as single-cell suspensions into 4–6 week old NSG mice (NOD/Shi-scid/IL-2R⁰ null; Charles River, France). Whenever animals showed neurological defects, enlarged abdomen or an s.c. growing tumour mass of $\sim 1000 \text{ mm}^3$, mice were sacrificed and tumour material was dissected. Xenograft tumours were stored in liquid nitrogen for future implantation or fixed in formalin. For storage in liquid nitrogen, single-cell suspensions of xenograft tumours were prepared by mechanical dissection after removal of macroscopically visible necrotic parts of the tumour and stored in 90% FCS, 10% DMSO in aliquots of 5×10^6 cells/ml in liquid nitrogen [31]. Secondary implantations were carried out after the depletion of mouse cells (#130-104-694, Miltenyi Biotec, Bergisch Gladbach, Germany) [32]. A PDX was defined as established when regrowth from xenograft tumour tissue stored in liquid nitrogen and stable growth over at least three transplantation passages was achieved.

Lymphoma dissemination of established models according to different implantation routes

Mouse-cell depleted human lymphoma cells from established PDX were injected i.c., i.s., or s.c. in 4–6 week old NSG mice (Charles River, France). Lymphoma cell dissemination was analysed by immunohistochemistry (IHC) and flow cytometry in the brain, eyes, spleen, liver, bone marrow (femur) and subcutaneous tumours after s.c. implantation (Figure 1).

Histology/immunohistochemistry

Tissues of interest were collected immediately after the euthanasia of the donor animal and fixated in 10% neutral buffered formalin for 24 h followed by routine processing and embedding into paraffin. The whole brain was cut into 2 mm thick slices with a special focus on macroscopically suspicious areas and then fixated and embedded into paraffin. Tissue sections of the brain, spleen, liver, femur and eyes including the retina and optic nerve were evaluated by light microscopy (Olympus, Model BX41 TF, Hamburg, Germany) after staining with haematoxylin and eosin (HE) using standard protocols.

For IHC: 2- μm -thick sections were cut from paraffin-embedded tissue specimens followed by routine processing. Patient and corresponding engrafted tumour tissue was stained using antibodies from Agilent Technologies, Waldbronn, Germany for BCL2 (clone 124, code IR61461) BCL6 (clone PG-B6p, code IR62561), MUM1 (clone MUM1p, code IR64461), CD10 (clone 56C6, code IR64861), CD19 (clone LE-CD19, code IR64861), CD79a (clone JCB117, code IR62161), Ki-67 (clone MIB-1, code IR62661-2), from Roche, Mannheim, Germany for PD-L1 (VENTANA PD-L1 [SP263]) and from abcam, Cambridge, UK, for c-Myc (clone Y69, ab168727). For the (host dependent) streptavidin-biotin-based peroxidase detection, EnVision Flex Peroxidase-Blocking Reagent (DAKO, SM801), EnVision Flex+ Rabbit (LINKER) (DAKO, K8019) or EnVision Flex+ Mouse (LINKER) (DAKO, K8021) and EnVision Flex/HRP (DAKO, SM802) from Agilent Technologies, Waldbronn, Germany, were used. Representative images of lymphoma infiltration of the brain, spleen, liver, bone marrow and eyes were taken with different magnifications using an Olympus, Model BX41 TF microscope (Hamburg, Germany) and Leica DFC450 digital microscope camera (Hamburg, Germany).

Flow cytometry analysis

The BD FACSCanto II Flow Cytometer and FACS Aria III (BD Biosciences, Heidelberg, Germany) were used for analysing and sorting. Cell suspensions from CNS, spleen and liver from i.s. PDX were incubated with the following fluorescence-labelled anti-human antibodies (BD Biosciences, Frankfurt am Main, Germany): CD45 FITC (560976), CD14 PE (557154), CD19 PE (561741), CD5 FITC (561896), CD20 FITC (560962), CD10 PE (557143), kappa FITC

TABLE 1 Patient characteristics of the four PCNSL, four SCNSL and two systemic DLBCL patients with established PDX models.

PDX no	Age	Time to CNS relapse (mts)	Histology/COO	Sex	ECOG	Ann-arbor stage, IPI, extra-nodal organ manifestations at first diagnosis	CNS prophyl-axis	CNS relapse with or without systemic relapse	Treatment at time of first diagnosis	Treatment at time of relapse	Follow-up (mts) after start of initial treatment and survival status
2922	75	NA	PCNSL/DLBCL/Non-GCB	f	1	IE, parenchymal lesion, no meningeal lesion or PVRL	NA	No	2× R-MTX-AraC, HCT-ASCT	NA	71 alive
4113	67	NA	PCNSL/DLBCL/GCB	m	1	IE, parenchymal lesion, no meningeal lesion or PVRL	NA	No	2× R-MTX-AraC, HCT-ASCT	NA	42 alive
4031	74	NA	PCNSL/DLBCL/Non-GCB	f	1	IE, parenchymal and meningeal lesion, no PVRL	NA	No	2× R-MTX-AraC, HCT-ASCT	NA	55 alive
4282	70	NA	PCNSL/DLBCL/Non-GCB	f	1	IE, parenchymal lesion, no meningeal lesion, no PVRL	NA	No	2× R-MTX-AraC, HCT-ASCT	NA	19 alive
2835	71	4	SCNSL/DLBCL/Non-GCB	m	3	IVA, 5/5, PUL, PLE, PER CNS-IPI: 5/6	2× HD-MTX	CNS parenchymal lesion, no meningeal or systemic lesions	6× R-CHOP, 2× R-MTX, 2× R	Focal RT 30 Gy, TMZ	8 dead
2958	61	72	SCNSL/DLBCL/Non-GCB	f	1	IIISEB, 3/5, concha nasalis, spleen CNS-IPI: 3/6	HCT-ASCT	CNS parenchymal lesion, no meningeal or systemic lesions	6× R-CHOP, 2× R, 3× R-ICE, HCT-ASCT	3× R-MTX-AraC-TT	77 dead
2972	70	18	SCNSL/DLBCL/Non-GCB	f	2	IVA, 4/5, mamma, MAR, OSS CNS-IPI: 4/6	2× HD-MTX	Meningeosis lymphomatosa, systemic lesions (spleen, LN, MAR), no CNS parenchymal lesion	6× R-CHOP, 2× R-MTX	1× R-MTX-AraC	20 dead
2938	57	5	SCNSL/DLBCL ^a	m	1	IVB, 4/5, MAR, PB, right testis CNS-IPI: 4/6	2× HD-MTX	Meningeosis lymphomatosa, no CNS parenchymal or systemic lesions	6× R-CHOP, 2× R-MTX	1× R-MTX-AraC-TT	7 dead
4009	50	NA	DLBCL/Non-GCB	f	1	IIIB	No	No	8× R-CHOP	R-DHAP	24 dead
4289	81	NA	DLBCL/Non-GCB	f	1	IIA, 2/5, no extranodal Manifestations	No	No	3× R-CHOP	NA	6 alive

Note: Ara-C=Cytarabine, COO = cell of origin, CNS = central nervous system, DLBCL = diffuse large B-cell lymphoma, f = female, HCT-ASCT = high dose chemotherapy and autologous stem cell transplantation, HD-MTX = high dose Methotrexat, IPI = international prognostic index, LN = lymph node, m = male, MAR = bone marrow, mts = months, NA = not applicable, Non-GCB=Non-germinal center B cell-like, R-CHOP = rituximab, cyclophosphamid, vincristine, prednisone, R-DHAP = rituximab, dexamethasone, cytarabine, cisplatin, R-ICE = rituximab, ifosfamid, carboplatin, etoposid, TT = thiotepa, OSS = bone, PB = peripheral blood, PCNSL = primary CNS lymphoma, PDX = patient-derived xenograft, PER = peritoneal, PLE = pleural, PUL = pulmonary, PVRL = primary vitreo retinal lymphoma.

^aNo biopsy was done, PDX establishment from CSF, 2938 PDX COO Classification: Non-GCB.

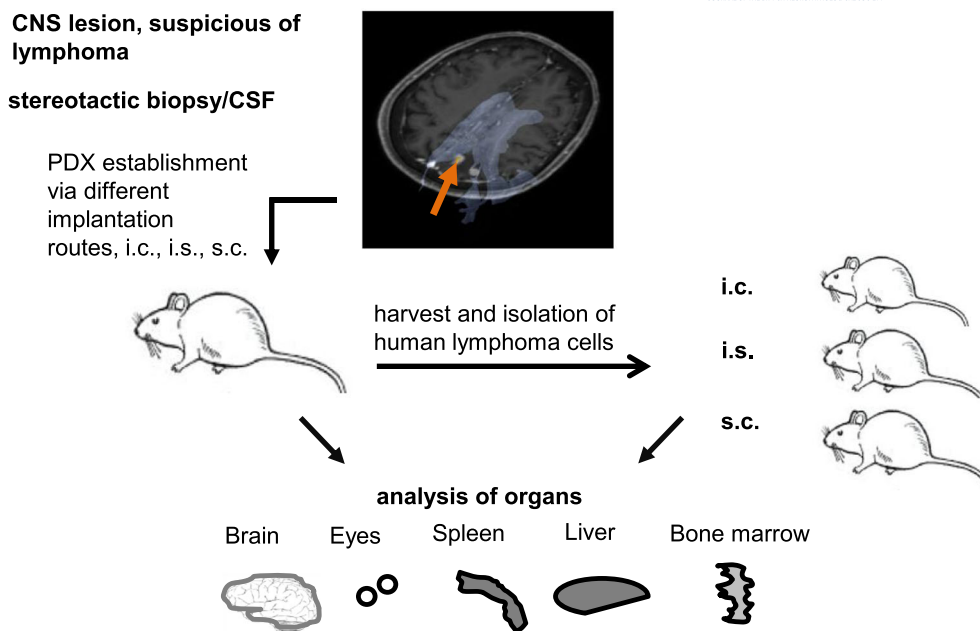


FIGURE 1 Workflow for the establishment of patient-derived xenograft (PDX) mouse models from PCNSL and SCNSL patient samples. In the MRI with reconstruction from a patient in the study, the orange arrow indicates lymphoma manifestation before stereotactic sampling. Patient samples, either stereotactic CNS biopsies or CSF, were implanted via different routes, intracerebral (i.c.), intrasplenic (i.s.) or subcutaneous (s.c.) into NSG recipient mice. Mice were sacrificed when neurologic symptoms or deterioration of overall condition occurred and cells from the brain, spleen or subcutaneous tumours were harvested and organs analysed for lymphoma infiltration. After mouse cell depletion, human lymphoma cells were re-implanted s.c. or i.s. into recipient mice. This procedure was repeated over several passages until stable growth was observed. Passaged human lymphoma cells were frozen in DMSO and stored. Subsequently, PDX lymphoma cells from these stocks were serially implanted orthotopically (i.c.) or heterotopically (i.s., s.c.) into NSG mice and the organs brain, eyes, spleen, liver and bone marrow (femur) were analysed for lymphoma infiltration.

(643773), lambda FITC (346600), CD200 PE (562125), CD184 PE (551510), CD44 PE (561858), CD54 PE (560971), or isotype control.

Fluorescence in situ hybridisation (FISH) and targeted next-generation sequencing

The slides were pretreated and hybridised with DNA Probes: XL DLEU/TP53, XL CDKN2A, XL IGH BA, XL BCL2 BA, XL BCL6 BA, XL MYC BA, XL ATM/11cen, XL t(11;14) MYEOV/IGH DF (MetaSystems, Altlußheim, Germany). Digital images of interphase spreads were recorded with a Sensys digital camera (Photometric, Tucson, AZ) on an Axioplan I fluorescence microscope (Zeiss, Jena, Germany).

The Illumina TruSight Lymphoid Sequencing Panel, including 40 genes (Table S2b) was used for targeted sequencing as described previously [33].

Cell culture and cytokine array

A single cell suspension was prepared from the spleen of i.s. PDX models with tumour content >95%. After 24 h of culture at 37° C, cell culture supernates were analysed for selected human cytokines and chemokines (Proteome Profiler Array ARY005B, R&D Systems, Wiesbaden, Germany).

RNA isolation and RNA sequencing

Total RNA was isolated from fresh, hCD19 sorted lymphoma cells (high pure RNA Isolation Kit, Roche Life Science, Mannheim, Germany) and quality and quantity were controlled using Qubit and fragment analyser technology (Thermo Fisher Scientific, Schwerte, Germany). For library preparation, RNA was converted to cDNA and amplified (10 PCR cycles) with the SMART Seq v4 ultra-low RNA kit (Takara, Saint-Germain-en-Laye, France, Land). Subsequently, two pools consisting of seven libraries each were sequenced on a HiSeq 4000 (Illumina Inc., San Diego, CA) in 100 bp paired-end mode, producing an output of at least 48 Mio. paired-end reads per sample.

RNA sequencing data are available on Gene Expression Omnibus under the accession number GSE189822 (using the token ofoxiyyaznsnhj) and GSE218285 (using the token crojuqewtjqfrub).

Bioinformatics and statistics

After adapter- and bad quality-trimming using Trimmomatic (v0.38), paired-end reads were aligned to the human genome and the read count per gene was quantified using STAR (v2.7.0a) [34, 35]. Read counts were further processed with R (v 4.2.1). Differential gene expression analysis was performed with edgeR package (v 3.38.4) in combination with SVA (v 3.44.0) to homogenise the two batches of

eight and four samples [36, 37]. Gene-set enrichment analysis was performed with the clusterProfiler R package (v 4.4.4) [38]. Gene sets from MsigDB (v7) [39] were used with a threshold of an adjusted p value <0.05 for significance. We used GraphPad version 5.3 (GraphPad Software, San Diego, USA) to generate Kaplan Meier analyses (log-rank tests, p value <0.05 ; progression-free survival [PFS]: time from first diagnosis to disease progression or death; overall survival [OS]: time from first diagnosis to death).

RESULTS

Establishment of primary and secondary CNS lymphoma PDX models

Stereotactic CNS biopsies were obtained from 10 patients with PCNSL and six patients with SCNSL. CSF samples were taken from one PCNSL and two SCNSL patients. Four lymph node biopsies and one bone marrow aspiration were obtained from five patients with systemic DLBCL without CNS manifestation. All 24 patients were under diagnostic work-up at the time of first diagnosis (PCNSL), at the time of first CNS relapse (SCNSL) or either at first diagnosis or relapse (systemic DLBCL) (Table 1, Table S1 and Figure S1).

In the first series, lymphoma cell implantation was performed via the s.c. route derived from seven patients [40]. After s.c. implantation, two out of three SCNSL samples engrafted at the site of implantation but only one out of four PCNSL biopsies engrafted. Interestingly, the successfully engrafted PCNSL animal developed a distended abdomen and after autopsy, intrasplenic lymphoma was detected, whereas no lymphoma cells were present at the s.c. site. Intracerebral implantation led to engraftment at the implantation site in five out of seven PCNSL CNS biopsies (71%) and three out of four SCNSL CNS/CSF biopsies (75%). Based on reports of successful engraftment of chronic lymphocyte leukaemia cells via intrasplenic implantation [41] and our observation that s.c. PCNSL implantation led to intrasplenic lymphoma prompting us to pursue the i.s. implantation route with successful engraftment of one SCNSL sample. Four of the five systemic DLBCL samples were implanted via the i.s. route and led to the successful engraftment of two samples; one biopsy derived from bone marrow infiltration was implanted i.t. but did not lead to engraftment (Figure S2).

Successfully engrafted lymphoma cells derived from subcutaneous, splenic or cerebral manifestations in xenotransplanted mice were isolated and serially reimplanted s.c. and i.s. over at least three passages to ensure stable growth. Four PCNSL (PDX 2922, PDX 4031, PDX 4113, PDX 4282) models, four SCNSL (PDX 2835, PDX 2938, PDX 2958, PDX 2972) models and two systemic DLBCL (PDX 4009, PDX 4289) models were successfully established.

Subcutaneous tumour sections of the PCNSL and SCNSL PDX models were further analysed by IHC using the “Hans classifier” panel [42], comprising CD10, BCL6 and MUM1 as well as CD20, CD79a and BCL2, and compared with the original patient brain biopsy. The

PDX models showed an almost identical marker profile in comparison to the original patient biopsy (Figure 2). Additionally, we stained for c-MYC, Ki-67 and PD-L1 showing largely concordant expression in PDX and corresponding patient biopsies (Table S3).

Dissemination pattern of lymphoma cells derived from established PDX models after secondary orthotopic or heterotopic implantation

The established PCNSL and SCNSL PDX models were used to trace lymphoma cell spreading in vivo (Figure 1). After orthotopic i.c. implantation, the PCNSL PDX showed strong lymphoma infiltration of the brain and eyes (Figure 3A). Of note, small lymphoma infiltrates emerged in the spleen, liver and bone marrow, demonstrating systemic dissemination. Similarly, the SCNSL PDX showed prominent lymphoma infiltration of the brain and eyes as well as small lymphoma infiltrates in the spleen, liver and bone marrow. The detection of prominent lymphoma infiltration surrounding the optic nerve suggests that most of the eye infiltration originated from the brain and meninges via continuous growth along the optic nerve sheath in both PCNSL and SCNSL PDX models (Figure 3A). Overall i.c. implantation resulted in strong lymphoma growth within the brain and eyes and minor systemic dissemination with no significant difference between PCNSL and SCNSL PDX models.

After heterotopic i.s. implantation, PCNSL and SCNSL PDX showed massive spleen infiltration as well as lymphoma infiltration of various degrees in liver and bone marrow (Figure 3B). Importantly, dissemination to the brain was detected in all three PCNSL and two out of three SCNSL cases, and was most pronounced in PDX 2922 and 4031 (PCNSL), and PDX 2958 (SCNSL). SCNSL PDX 2972 in addition to brain manifestation showed massive bone marrow infiltration (Figure 3B), also observed in the corresponding patient. Importantly, i.s. implantation of a PDX established from bone marrow from the same patient again resulted in massive infiltration of spleen and bone marrow, but consistently no lymphoma cells were detected in CNS parenchyma, meninges or retina (data not shown). We next analysed two PDX models derived from lymph node biopsies from two DLBCL patients without a history of synchronous or metachronous secondary CNS manifestation. In contrast to PCNSL and SCNSL PDX models, the systemic DLBCL PDXs (4009 and 4289) after i.s. implantation showed massive infiltration of the spleen and infiltration of bone marrow, but no lymphoma infiltration in the brain or eyes (Figure 3B). When we analysed s.c. implantation, lymphoma growth was observed at the s.c. implantation site, whereas only single cell infiltrates were detected in the liver, bone marrow, spleen and CNS with no differences between PCNSL and SCNSL PDX. Only one PCNSL PDX (PDX 4031) showed lymphoma infiltrates $>10\%$ in the brain and liver after s.c. implantation (Figure S3). Together, these data demonstrate that after heterotopic i.s. implantation, primary and secondary CNS lymphoma PDX, but not systemic lymphoma PDX display dissemination to the brain and eyes.

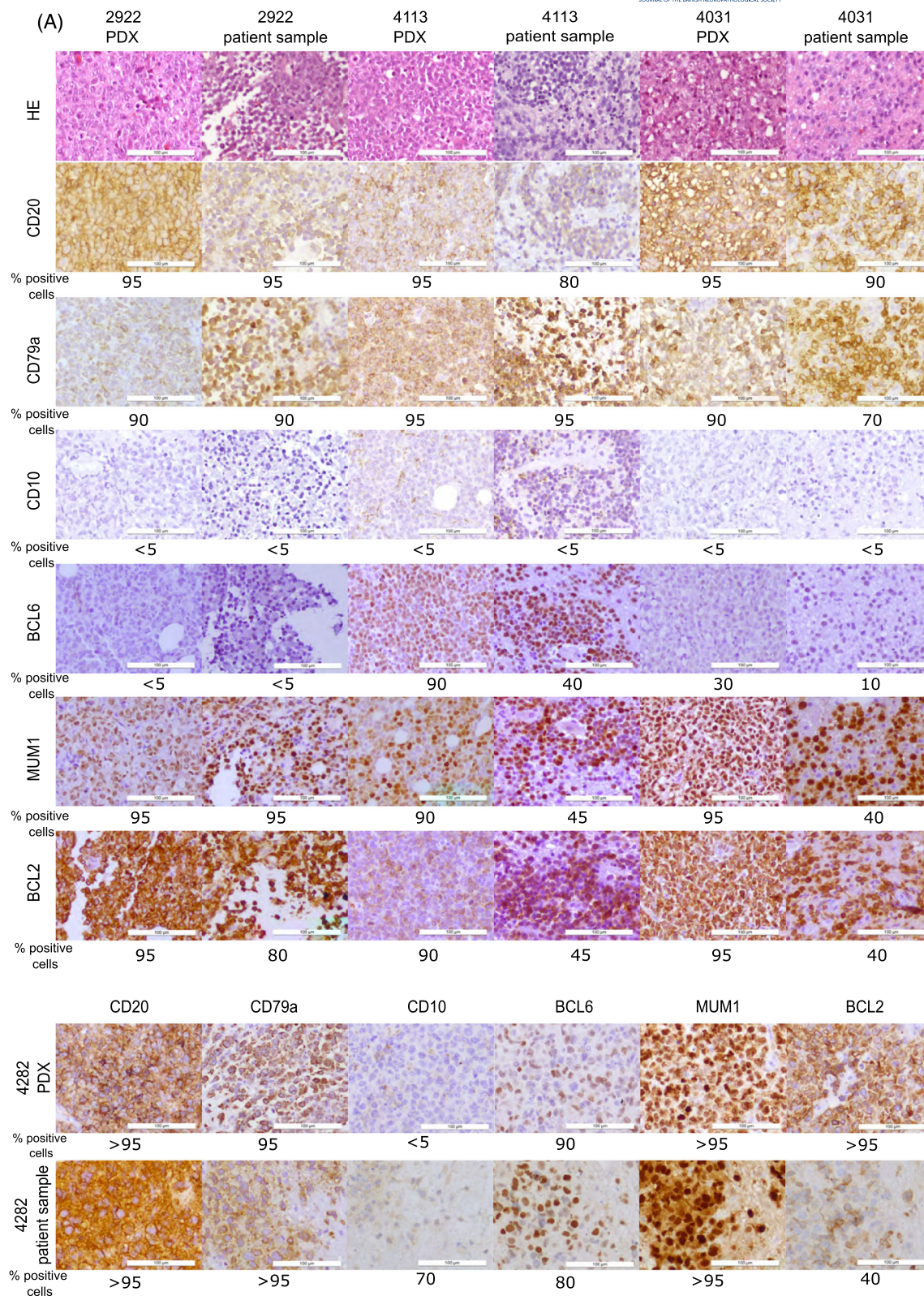
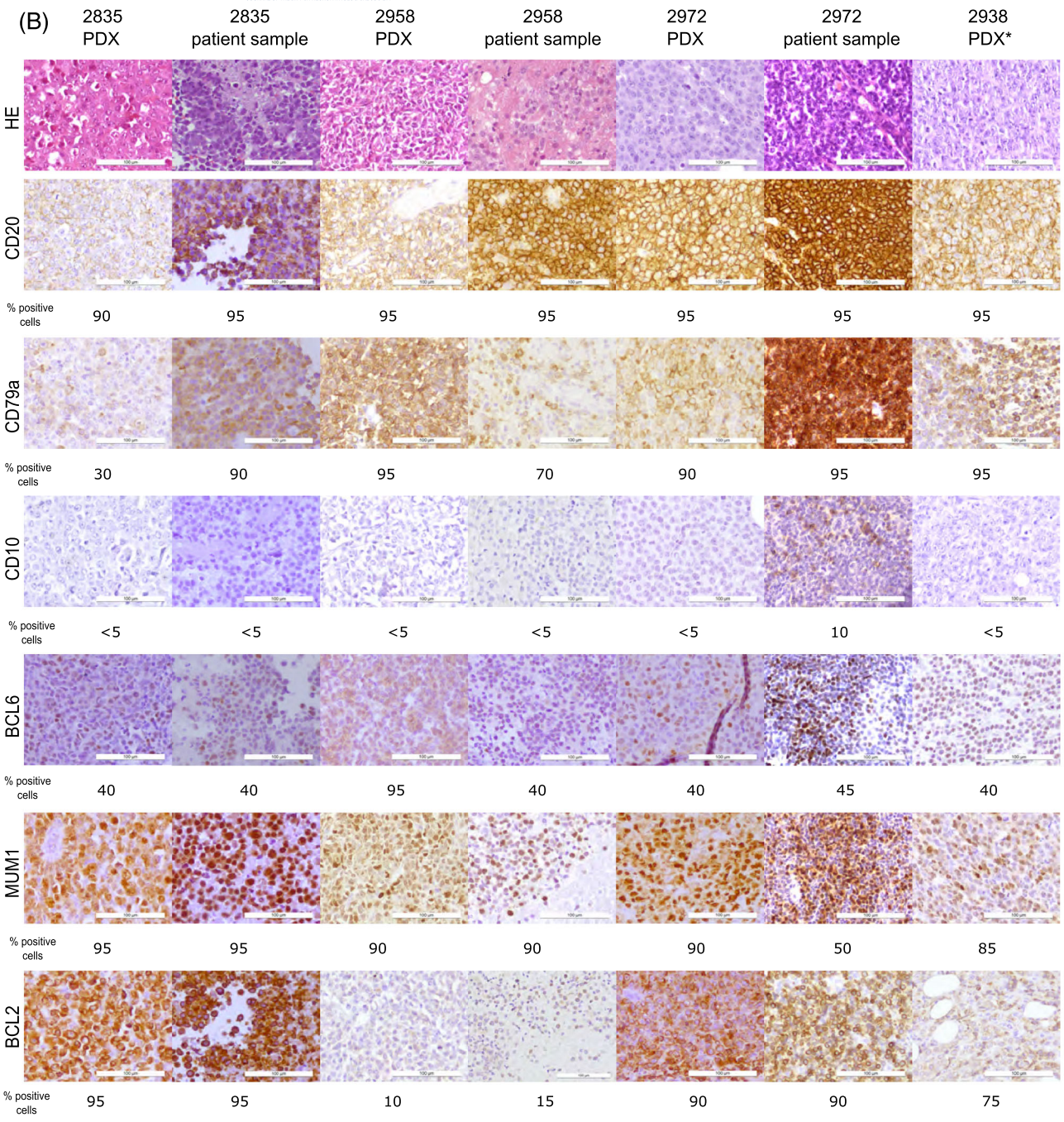


FIGURE 2 (A,B) Characterisation of PDX models by histology and immunohistochemistry. Subcutaneous tumour sections of the four PCNSL (A) and four SCNSL (B) PDX models were analysed by histology and immunohistochemistry using a panel of immunohistochemical markers (CD20, CD79a, CD10, MUM1, BCL2 and BCL6). Compared with the original patient samples, PDX lymphomas showed a largely identical immunophenotypic profile. The cell of origin classification was determined according to the Hans classifier. In one case of SCNSL PDX (2938), the generation of the PDX model was started from CSF and no initial biopsy was taken. Scale bars, 100 μ m. Each IHC antibody stain was evaluated by two pathologists (S.D. and H.E.S.) through visual estimation. Positive cells in percentage with 5% increments are given for each case. For Hans classifier markers percentages $\geq 30\%$ are considered positive.



*PDX was established from CSF, no brain biopsy was taken

FIGURE 2 (Continued)

Retinal infiltration mimics PVRL

Infiltration of the eyes was detected in the choroid in two SCNSL PDX models, whereas infiltration of the retina was only detected in one PCNSL, PDX 4031 (Figure 3B). To investigate the detailed eye infiltration patterns, PCNSL PDX model 4031 and SCNSL PDX model 2958 were implanted i.s. into 13 recipient mice. IHC analysis detected PCNSL PDX 4031 lymphoma infiltration in the retina but not in the optic nerve in nine out of 13 animals thus mimicking PVRL. Four out of 13 animals

showed no eye infiltration. SCNSL PDX model 2958 showed no retinal lymphoma infiltration in 13 out of 13 cases (Figure 4).

Flow cytometric, molecular genetic and cytokine secretion profiling of PDX organ lymphoma infiltrates

To further characterise lymphoma spreading after i.s. implantation, we analysed the spleen, liver and brain of two PCNSL and one SCNSL

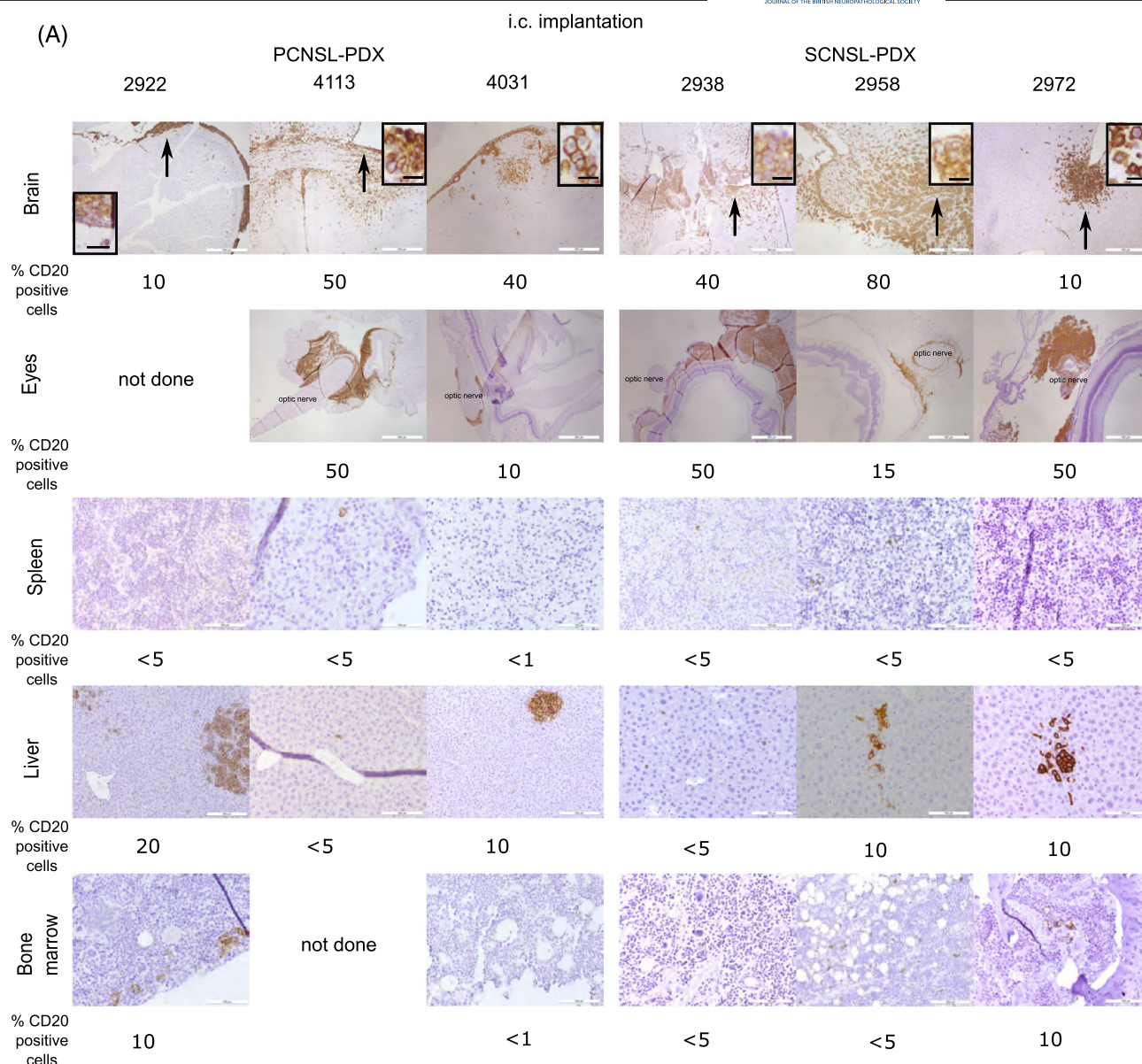


FIGURE 3 (A,B) CD20 staining of different organs after secondary i.c. (A) or i.s. (B) implantation of PDX lymphoma cells into NSG recipient mice ($N = 3$). After i.c. (A) implantation, the PCNSL and SCNSL PDX showed strong lymphoma infiltration of the brain and eyes. In addition, small lymphoma infiltrates in the spleen, liver and bone marrow were detectable. After i.s. (B) implantation, the PCNSL PDX showed massive spleen infiltration, as well as lymphoma infiltrates in the liver, bone marrow, brain and in one case infiltration of the retinal pigment epithelium (RPE) (PDX 4031). The SCNSL PDX differed in having less brain and bone marrow infiltration and infiltration of the eyes (two cases) was localised in the choroid, whereas no infiltration of the RPE was detected. As a control group 2 systemic DLBCL PDX 2009 and 4289 were implanted i.s. in five recipient mice. No lymphoma infiltration of CNS and eyes was detected, whereas lymphoma infiltrates in the spleen, liver and bone marrow were observed. Representative images of slides were selected. Bar scale 100 μm , except brain and eye panel in a and brain panel in b bar with scale 500 μm . Higher magnification inserts are included in selected images with positive lymphoma cells, bar scale 12 μm . Visual estimation of the percentage of infiltration in the respective organs was performed by two pathologists (S.D., H.E.S). For each PDX, at least three slides were analysed, representative slide sections were selected and infiltration percentages were documented in 5% increments. Below 1 means no positive cells were detected in the three analysed slides.

PDX model via flow cytometry. PCNSL PDX 4113 showed human CD19⁺ cells with kappa light chain restriction, corresponding to the originating tumour as well as expression of the cell adhesion molecules CXCR4 (CD184), ICAM1 (CD54) and HCAM (CD44) in spleen, liver and brain (Figure S4a,b). PCNSL PDX 4031 showed human CD19⁺ cells with lambda light chain restriction corresponding to

originating tumour as well as expression of cell adhesion molecules CXCR4 (CD184), ICAM1 (CD54) and HCAM (CD44) in spleen, liver and brain (data not shown). SCNSL PDX 2958 showed human CD19⁺ cells with kappa light chain restriction corresponding to originating tumour as well as expression of cell adhesion molecules CXCR4 (CD184), ICAM1 (CD54) and HCAM (CD44) in spleen, liver and brain

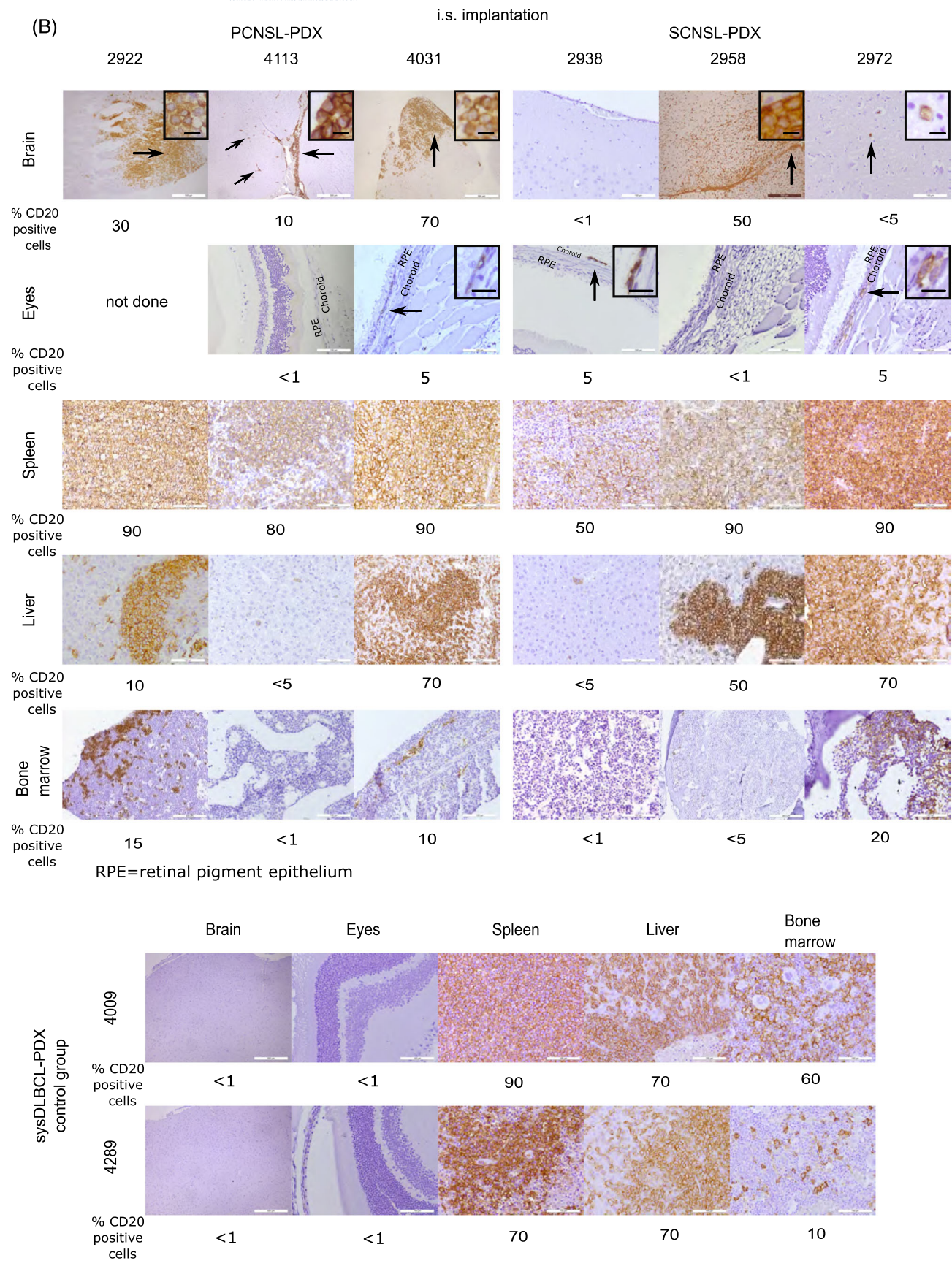


FIGURE 3 (Continued)

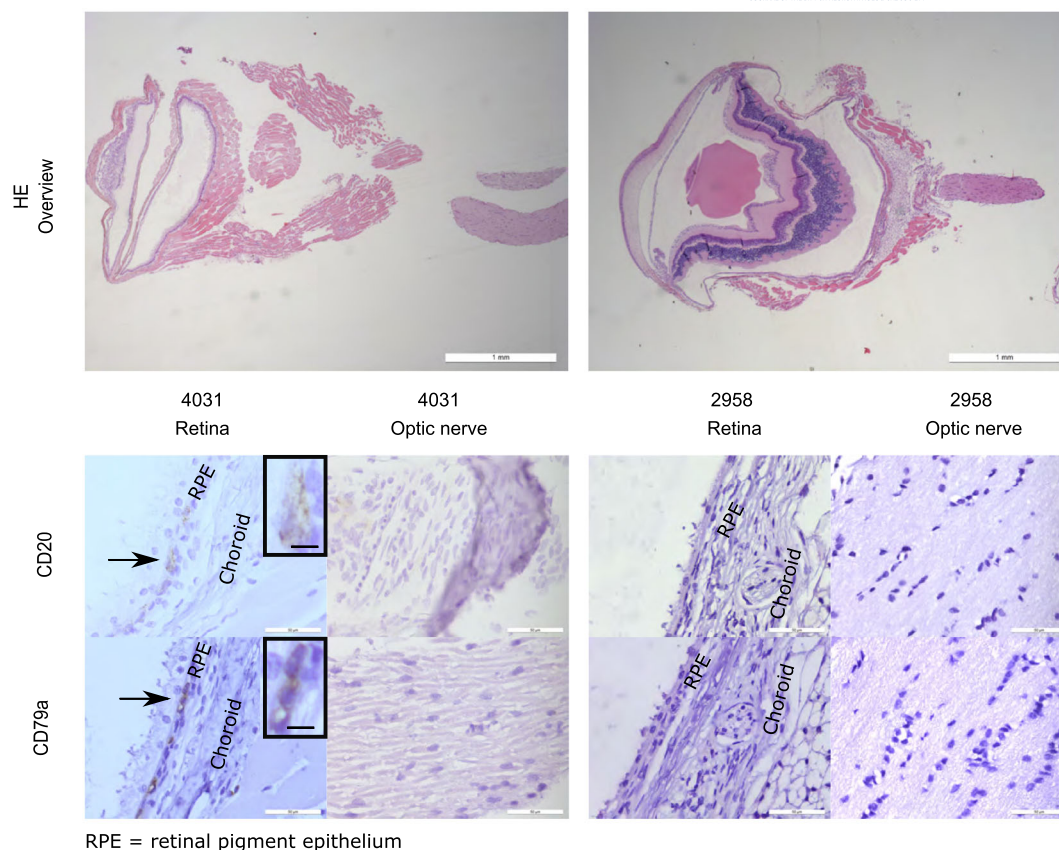


FIGURE 4 Eye infiltration pattern of PCNSL PDX model 4031. A total of 13 recipient mice were implanted intrasplenically with lymphoma cells from PCNSL PDX model 4031. Nine out of 13 mice showed lymphoma infiltration in the retinal pigment epithelium (RPE), but not in the optic nerve, whereas 4 out of 13 mice did not show any lymphoma infiltration in any part of the eyes. As a control group, 13 mice were implanted with lymphoma cells from SCNSL PDX model 2958. In these mice, no lymphoma infiltration of any part of the eye was detected. Bar scale in HE overview image 1 mm, CD20 and CD79a images 50 μ m, bar scale in inserts 12 μ m.

(data not shown). Both PCNSL PDX models were analysed with FISH (Figure S5). PCNSL PDX 4031 showed loss of X chromosome, *TP53* deletion, deletion of 14q32/*IGH* and deletion of 9p21/*CDKN2A*. PCNSL PDX 4113 showed biallelic deletion of 9p21/*CDKN2A*. None of the PDX showed aberrations in *cMYC*, *BCL2*, *BCL6* or 11q22/*ATM* (Figure S5). Sequencing of both PCNSL PDX revealed *MYD88*^{L265P} mutations in both PCNSL PDX as well as a *CD79A* mutation in PDX 4113 (Table S2a,b).

To assess cytokine secretion profiles of organ infiltrating PDX lymphoma cells, isolated spleen xenograft lymphoma cells of PCNSL PDX 4031 and SCNSL PDX 2958 were cultured and supernatants were analysed by cytokine array. In supernatants of PCNSL PDX 4031, migration inhibitory factor (MIF) and the macrophage inflammatory proteins MIPalpha and beta were detected whereas SCNSL PDX 2958 cells secreted MIF, IL-16, IL-6, IL-10 and CXCL10/IP-10 (Figure S6).

Transcriptome analysis of brain vs spleen lymphoma manifestations by RNAseq

RNAseq analysis of sorted lymphoma cells isolated from the brain after i.c. implantation or spleen after i.s. implantation of three PCNSL

PDX (4031, 4113, 4282) and three SCNSL PDX (2958, 2938, 2972) revealed major gene expression differences between PCNSL and SCNSL as expected (Figure 5A). In the principal component analysis differences between PCNSL and SCNSL PDX were more pronounced than differences between CNS and splenic manifestations of each PDX model (Figure 5B). Overall, 347 genes were expressed differently in the PCNSL CNS vs SCNSL CNS comparison, whereas 287 genes showed significant differential expression in the PCNSL spleen vs SCNSL spleen comparison (Figure 5C). The genes that were upregulated in PCNSL compared with SCNSL are involved in cell migration, cell adhesion processes, metastasis, cell proliferation, angiogenesis and DNA damage. Intergroup comparison between CNS and spleen in the PCNSL as well as the SCNSL group also identified significantly differentially expressed genes (Figure 5D,E). Genes that were highly expressed in CNS vs spleen in the PCNSL group included genes that are linked to the extracellular matrix, cell migration, brain development, cell energy and inflammatory processes (Figure 5D). Moreover, we identified a small overlap of commonly upregulated and downregulated genes in the CNS-spleen comparisons of both PCNSL and SCNSL with 11 genes upregulated and eight genes downregulated (Figure 5F,G). On the pathway level, epithelial-mesenchymal transition, inflammatory response, myogenesis and glycolysis were among

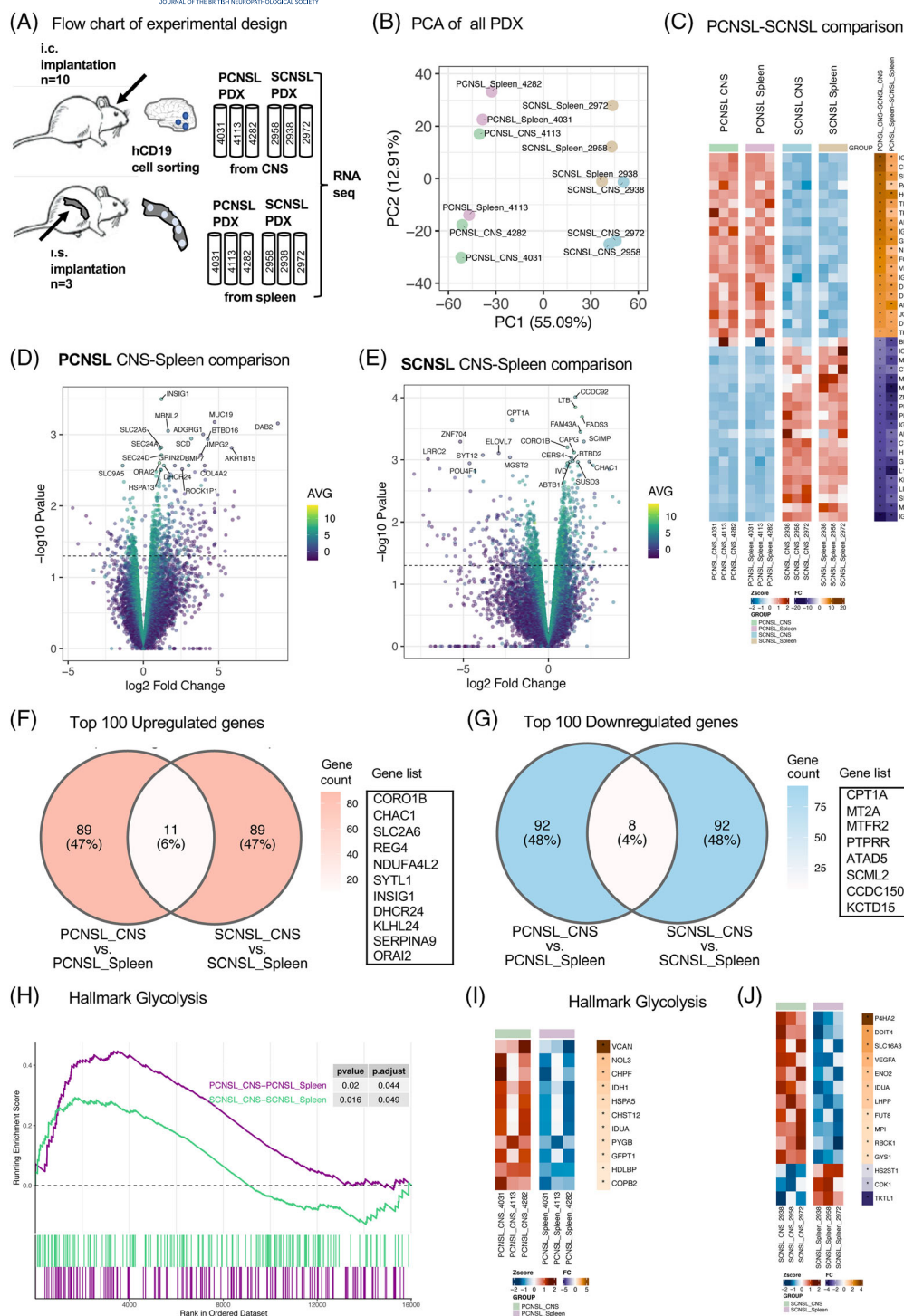


FIGURE 5 Transcriptomic analysis of PCNSL and SCNSL PDX. (A) Flow chart of the experimental approach. Human anti-CD19 stained flow-sorted lymphoma cells from CNS and spleen of three PCNSL PDX and three SCNSL PDX were subjected to RNAseq analysis. (B) Principal component analysis revealed distinct clustering for each PDX model (colour-coded, green: PCNSL CNS, purple: SCNSL spleen, blue: SCNSL CNS, orange: SCNSL spleen). (C) Heat map showing the 20 most differentially expressed genes in both PCNSL CNS vs SCNSL CNS and PCNSL spleen vs SCNSL spleen (adj. p value <0.05). (D) Volcano plot of differentially expressed genes of PCNSL lymphoma cells from CNS vs. spleen marking the top 25 differentially expressed genes. AVG represents the average normalised intensity across all samples from both conditions. (E) Volcano plot of differentially expressed genes of SCNSL lymphoma cells from CNS vs. spleen marking the top 25 differentially expressed genes. (F) Venn diagram showing the top 100 significantly upregulated genes of PCNSL CNS vs. spleen and SCNSL CNS vs. spleen comparisons. The 11 genes that overlap are listed. (G) Venn diagram showing the top 100 significantly downregulated genes of PCNSL CNS vs. spleen and SCNSL CNS vs. spleen comparisons. The eight genes that overlap are listed. (H) Gene-set enrichment plot for Hallmark glycolysis pathway, potentially relevant for PCNSL and SCNSL pathogenesis. (I, J) Hallmark pathway glycolysis gene sets showing significantly regulated genes (p value <0.05) in the PCNSL CNS vs spleen comparison (I) and SCNSL CNS vs spleen comparison (J).

the most significantly upregulated hallmark pathways in PCNSL CNS vs spleen comparison whereas TNFA signalling via NFkB, inflammatory response and glycolysis were among the most significantly upregulated hallmark pathways in SCNSL CNS vs spleen comparison (Figure S7). The hallmark glycolysis pathway was significantly upregulated in both PCNSL and SCNSL CNS vs spleen comparison (Figure 5H–J).

DISCUSSION

Unravelling the molecular pathways that contribute to PCNSL and SCNSL tropism to neural tissue has been hampered by a lack of suitable *in vivo* models. In this study, we established a patient-derived PDX mouse model that preserves the lymphoma (DLBCL) cell phenotype of the corresponding patient CNS biopsies after serial transplantation and allows (1) to study lymphoma cell dissemination after both orthotopic and heterotopic implantation and (2) to analyse cellular and molecular features of lymphoma manifestations in different organs (CNS vs non-CNS).

The establishment of patient-derived PCNSL and SCNSL xenograft mouse models via orthotopic implantation into the CNS has been reported [29, 30]. Like in our model, the lymphoma cells expanding in recipient mice showed the same immune-histological phenotype compared with patient biopsies. In contrast to reported patient-derived PCNSL PDX models, we, for the first time, report heterotopic, such as intrasplenic, implantation strategies to study the lymphoma cell fate of both PCNSL and SCNSL in comparison to systemic DLBCL without CNS manifestations as a control group. We observed systemic dissemination in the spleen, liver and bone marrow in SCNSL and systemic DLBCL PDX but surprisingly also in the PCNSL PDX. This observation supports the hypothesis of recirculation of transformed B-cells between the systemic and CNS compartment with clinical CNS manifestation occurring due to a highly selective CNS tropism [25, 26]. Although PCNSL patients display clonal B-cells in the circulation [8, 9], the overt systemic spread to other organs observed in our model does not occur in PCNSL patients and may be due to the immunodeficient host state of the recipient mice affecting immune-mediated PCNSL lymphoma cell elimination in the periphery. In addition, we observed lymphoma cells spreading to the brain and eyes after intrasplenic implantation of both PCNSL and SCNSL-derived PDX models, but not in PDX derived from systemic DLBCL without CNS manifestations. Notably, the PCNSL lymphoma infiltration of the eye in this model (which occurred in 69% of *i.s.* transplants of PCNSL PDX model 4031) was limited to the retina and did not affect other eye compartments such as the optic nerve, which closely models PVRL at early stages of the disease [2]. This is in contrast to previously reported PVRL mouse models established by injecting B-lymphoma cells or cell lines into the eye [43, 44] which resulted in massive infiltration of most parts of the eye. The PVRL infiltration pattern was observed only in *i.s.* PCNSL xenografted mice. PVRL lymphoma cells in this model expressed chemokine receptors CXCR4 and CXCR5 as well as CD44 [45].

FISH analysis and sequencing of PDX lymphoma cells detected mostly well-known PCNSL and SCNSL alterations, notably *CDKN2A* deletions [46] and the *MYD88*^{L265P} mutation [47]. *IGH* deletions (PCNSL PDX 4031 and SCNSL PDX 2972) have been described by Montesinos-Rongen et al. in a cytogenetic study of 13 PCNSL patients in about 60% of cases [48]. *TP53* deletion (PCNSL PDX 4031) is a less common aberration [13]. Loss of X chromosome (PCNSL PDX 4031) has to our knowledge not been described in PCNSL, but sex chromosome abnormalities can occur in DLBCL and brain tumours [49, 50] and have been described to arise independent of haematologic disease with higher age [51]. Mutations in B-cell receptors are common alterations in PCNSL, especially the *CD79B* mutation [24, 52]. To our knowledge *CD79A* mutations (PCNSL PDX 4113), are not common in PCNSL, but have been described in systemic DLBCL [53].

Characterisation of established PDX models via flow cytometry as described for PCNSL stereotactic biopsies [54, 55] confirmed the conserved PCNSL immunophenotype of lymphoma cells in different organs including the CNS after *i.s.* implantation. In addition, we detected the expression of cell adhesion molecules ICAM1 (CD54) and HCAM (CD44) and the chemokine receptor CXCR4 in PCNSL PDX models 4031 and 4113 as previously described [56, 57]. CD44 is also expressed on astrocytes, microglia and cerebral endothelial cells [57] and interacts with osteopontin, an extracellular matrix molecule that was shown to be upregulated in PCNSL [58, 59]. He et al. associated increased expression of CD44 and CXCR4 with aggregated perivascular lymphoma cell formation, a characteristic histologic feature of PCNSL [60]. Interestingly, CD44 (via CD74) and CXCR4 are activated by MIF [61], which we found to be secreted by spleen-derived PCNSL PDX lymphoma cells. This interaction induces ERK1/2 phosphorylation leading to the release of pro-inflammatory cytokines associated with cell proliferation and tumour angiogenesis [39, 50], which might be involved in PCNSL pathogenesis and progression.

PCNSL PDX lymphoma cells were also found to release macrophage inflammatory protein 1α (MIP-1α) and 1β (MIP-1β). MIP-1α or CCL3 is a pro-inflammatory chemokine produced by many different cell types such as immune cells, epithelial cells, fibroblasts and glial cells and is known to play a role in cell adhesion and migration [62]. The interaction with its receptors CCR1 and CCR5 is important in mediating pro-survival effects in various haematologic neoplasms [63], and plays a role in multiple myeloma bone disease [64], but has not been described in the context of PCNSL.

The cytokines that we found to be secreted by spleen-derived SCNSL PDX 2958 lymphoma cells, notably IL-6 and IL-10 can be induced via activation of IRAK4 by the NFkB pathway, that in turn will be activated by the *MYD88*^{L265P} mutation [57] present in this model. A potential role for IL-10 in protecting lymphoma cells from immune reactions in the CNS has been discussed for PCNSL [65].

The heterotopic *i.s.* implantation model offered the opportunity to investigate transcriptomic differences between spleen and CNS manifestations for SCNSL and PCNSL PDX. We found large gene expression differences between PCNSL and SCNSL. More importantly, we identified specific gene sets that were significantly

upregulated or downregulated in PCNSL CNS vs spleen as well as in SCNSL CNS vs spleen comparison, defining distinct transcriptome signatures for both PCNSL and SCNSL in the CNS compartment. Regulated genes that shared up or downregulation in CNS vs spleen lymphoma cells originating from both PCNSL and SCNSL are potential candidates for a role in CNS lymphoma pathogenesis and tropism. Regenerating islet-derived type 4 (*REG4*) showed a 2.3-fold (PCNSL) and 3.5-fold (SCNSL) upregulation in CNS vs spleen lymphoma cells and has been described to promote invasion and migration of cancer cells in various human cancers [66]. Recently, *REG4* was found to interact with the CD44 receptor, which then can activate the transcription of pro-proliferative, pro-metastatic and anti-apoptotic genes [67]. Among the most significantly upregulated hallmark pathways in the PCNSL CNS vs spleen comparison were epithelial-mesenchymal transition, coagulation and myogenesis. We found *SPP1*, known to be involved in the pathogenesis of PCNSL, significantly upregulated in CNS vs spleen comparison and part of the hallmark epithelial-mesenchymal transition gene list [58, 68]. Moreover, we identified the glycolysis pathway as significantly upregulated in both PCNSL and SCNSL CNS vs spleen transcriptome analysis. In accordance, a recent study by Tateishi et al. identified the deregulation of the *RELA/p65* hexokinase 2 axis, involved in the glycolytic pathway as a driver of intracerebral lymphoma progression in an orthotopic PDX model of PCNSL [29].

Whether the observed transcriptome differences of PCNSL and SCNSL in different mouse tissues reflect adaption to the respective local microenvironment (brain vs spleen) or represent a gene expression signature involved in lymphoma cell migration to distinct sites cannot be discriminated from the obtained RNAseq data sets and needs to be further investigated by functional blockade or overexpression studies of candidate molecules or signalling pathways in the established PDX models.

In summary, we established the first patient-derived PCNSL PDX model that explores intrasplenic implantation and reveals lymphoma infiltration of the brain and retina mimicking PCNSL and PVRL. This model might be used to unveil genetic and molecular hallmarks of CNS lymphoma pathogenesis and progression and to explore targets for therapeutic intervention.

AUTHOR CONTRIBUTIONS

Nikolas von Bubnoff, Lisa Kristina Isbell, Cordula Tschuch and Julia Schueler were responsible for the conceptualisation of the study as well as for planning experiments, analysing data, interpreting results and writing the original draft. Peter Christoph Reinacher, Elisabeth Schorb, Florian Scherer, Lisa Kristina Isbell and Cordula Tschuch were responsible for project administration. Lisa Kristina Isbell, Cordula Tschuch, Silvia Waldeck, Khalid Shoumariyeh, Dorothee Lenhard, Ingrid Bartsch, Milena Pantic, Vinodh Kakkassery and Janaki Manoja Vinnakota performed experiments, analysed data and prepared figures. Soroush Doostkam, Hans Eckart Schaefer and Anna Verena Frey performed histology, immunohistology as well as molecular analysis. Geoffroy Andrieux and Melanie Boerries performed a bioinformatic analysis of RNAseq data. Nikolas von Bubnoff, Peter Christoph

Reinacher, Elisabeth Schorb, Melanie Boerries, Gerald Illerhaus, Justus Duyster and Julia Schueler supplied resources and patient data. All authors have reviewed, edited and finalised the manuscript.

ACKNOWLEDGMENTS

Nikolas von Bubnoff receives funding from the Deutsche Forschungsgemeinschaft (DFG) (Project ID: 386260575) and the German Federal Ministry of Education and Research (BMBF) within the OUTLIVE consortium (Project ID: 01KD2103A). Melanie Boerries is supported by the Deutsche Forschungsgemeinschaft (DFG) – CRC 850 subprojects C9 and Z1, CRC1479 (Project ID: 441891347-S1), CRC 1160 (Project ID 256073931-Z02), CRC1453 (Project ID 431984000 – S1) and TRR167 (Project Z01). We also acknowledge funding from the German Federal Ministry of Education and Research (BMBF) within the Medical Informatics Funding Scheme – MIRACUM-FKZ 01ZZ1801B (M.B.) and EkoEstMed-FKZ 01ZZ2015 (G.A.). We thank Dieter Herchenbach and Jan Bodinek-Wersing for cell sorting and Dietmar Pfeifer for sequencing. We thank Jonathan R Isbell and Juergen Lohmeyer for proofreading. Open Access funding enabled and organized by Projekt DEAL.

CONFLICT OF INTEREST STATEMENT

Nikolas von Bubnoff received research support from Novartis and honoraria from Novartis, Takeda and the Forum für Medizinische Fortbildung. Khalid Shoumariyeh received honoraria from Novartis, Blueprint Medicines and Pfizer. Peter C Reinacher receives research support from Else Kröner-Fresenius Foundation (Germany) and Fraunhofer Foundation (Germany), received personal honoraria for lectures or advice from Boston Scientific (USA) and Brainlab (Germany) and is a consultant for Boston Scientific (USA), Inomed (Germany) and Brainlab (Germany). The other authors have no competing interests to declare that are relevant to the content of this article.

INFORMED CONSENT STATEMENT

Informed consent was obtained from all subjects involved in the study.

DATA AVAILABILITY STATEMENT

The RNA sequencing data that support the findings of this study are openly available on Gene Expression Omnibus under the accession number GSE189822 (using the token ofoxiyyaznsnhj) and GSE218285 (using the token crojuqewtjqrub).

ETHICS STATEMENT

The study was conducted according to the guidelines of the Declaration of Helsinki, and approved by the Institutional Ethics Committee of the University Medical Center Freiburg (Number: 91/14_170606). All animal experiments were carried out in strict accordance with the recommendations in the Guide for the Care and Use of Laboratory Animals of the Society of Laboratory Animals (GV SOLAS) in an AAALAC-accredited animal facility. All animal experiments were approved by the Committee on the Ethics of Animal Experiments of the regional council (Permit numbers: G-18/78 and G17/138).

PEER REVIEW

The peer review history for this article is available at <https://publons.com/publon/10.1111/nan.12899>.

REFERENCES

- Ferreri AJ. How I treat primary CNS lymphoma. *Blood*. 2011;118(3):510-522. doi:10.1182/blood-2011-03-321349
- Chan CC, Rubenstein JL, Coupland SE, et al. Primary vitreoretinal lymphoma: a report from an International Primary Central Nervous System Lymphoma Collaborative Group symposium. *Oncologist*. 2011;16(11):1589-1599. doi:10.1634/theoncologist.2011-0210
- Kalogeropoulos D, Vartholomatos G, Mitra A, et al. Primary vitreoretinal lymphoma. *Saudi J Ophthalmol*. 2019;33(1):66-80. doi:10.1016/j.sjopt.2018.12.008
- Illerhaus G, Kasenda B, Ihorst G, et al. High-dose chemotherapy with autologous haemopoietic stem cell transplantation for newly diagnosed primary CNS lymphoma: a prospective, single-arm, phase 2 trial. *Lancet Haematol*. 2016;3(8):e388-e397. doi:10.1016/S2352-3026(16)30050-3
- Houillier C, Soussain C, Ghesquieres H, et al. Management and outcome of primary CNS lymphoma in the modern era: an LOC network study. *Neurology*. 2020;94(10):e1027-e1039. doi:10.1212/WNL.0000000000008900
- Ferreri AJ, Cwynarski K, Pulczynski E, et al. Chemoimmunotherapy with methotrexate, cytarabine, thiopeta, and rituximab (MATRix regimen) in patients with primary CNS lymphoma: results of the first randomisation of the International Extranodal Lymphoma Study Group-32 (IELSG32) phase 2 trial. *Lancet Haematol*. 2016;3:e217-e227.
- Ferreri AJM, Cwynarski K, Pulczynski E, et al. Whole-brain radiotherapy or autologous stem-cell transplantation as consolidation strategies after high-dose methotrexate-based chemoimmunotherapy in patients with primary CNS lymphoma: results of the second randomisation of the International Extranodal Lymphoma Study Group-32 phase 2 trial. *Lancet Haematol*. 2017;4:e510-e523.
- Fukumura K, Kawazu M, Kojima S, et al. Genomic characterization of primary central nervous system lymphoma. *Acta Neuropathol*. 2016;131(6):865-875. doi:10.1007/s00401-016-1536-2
- McCann KJ, Ashton-Key M, Smith K, Stevenson FK, Ottensmeyer CH. Primary central nervous system lymphoma: tumor-related clones exist in the blood and bone marrow with evidence for separate development. *Blood*. 2009;113(19):4677-4680. doi:10.1182/blood-2008-09-179366
- Boehme V, Schmitz N, Zeynalova S, Loeffler M, Pfreundschuh M. CNS events in elderly patients with aggressive lymphoma treated with modern chemotherapy (CHOP-14) with or without rituximab: an analysis of patients treated in the RICOVER-60 trial of the German High-Grade Non-Hodgkin Lymphoma Study Group (DSHNHL). *Blood*. 2009;113(17):3896-3902. doi:10.1182/blood-2008-10-182253
- Calimeri T, Lopodote P, Ferreri AJM. Risk stratification and management algorithms for patients with diffuse large B-cell lymphoma and CNS involvement. *Ann Lymphoma*. 2019;3:1-19. doi:10.21037/aol.2019.06.01
- Ferreri AJM. Secondary CNS lymphoma: the poisoned needle in the haystack. *Ann Oncol*. 2017;28(10):2335-2337. doi:10.1093/annonc/mdx515
- Chapuy B, Roemer MG, Stewart C, et al. Targetable genetic features of primary testicular and primary central nervous system lymphomas. *Blood*. 2016;127(7):869-881. doi:10.1182/blood-2015-10-673236
- Chapuy B, Stewart C, Dunford AJ, et al. Molecular subtypes of diffuse large B cell lymphoma are associated with distinct pathogenic mechanisms and outcomes. *Nat Med*. 2018;24(5):679-690. doi:10.1038/s41591-018-0016-8
- Schmitz R, Wright GW, Huang DW, et al. Genetics and pathogenesis of diffuse large B-cell lymphoma. *N Engl J Med*. 2018;378(15):1396-1407. doi:10.1056/NEJMoa1801445
- Wright GW, Huang DW, Phelan JD, et al. A probabilistic classification tool for genetic subtypes of diffuse large B cell lymphoma with therapeutic implications. *Cancer Cell*. 2020;37:551-568.
- Lacy SE, Barrans SL, Beer PA, et al. Targeted sequencing in DLBCL, molecular subtypes, and outcomes: a Haematological Malignancy Research Network report. *Blood*. 2020;135(20):1759-1771. doi:10.1182/blood.2019003535
- Alizadeh AA, Eisen MB, Davis RE, et al. Distinct types of diffuse large B-cell lymphoma identified by gene expression profiling. *Nature*. 2000;403(6769):503-511. doi:10.1038/35000501
- Klanova M, Sehn LH, Bence-Bruckler I, et al. Integration of cell of origin into the clinical CNS International Prognostic Index improves CNS relapse prediction in DLBCL. *Blood*. 2019;133(9):919-926. doi:10.1182/blood-2018-07-862862
- Lenz G, Wright GW, Emre NC, et al. Molecular subtypes of diffuse large B-cell lymphoma arise by distinct genetic pathways. *Proc Natl Acad Sci U S A*. 2008;105(36):13520-13525. doi:10.1073/pnas.0804295105
- Braggio E, Van Wier S, Ojha J, et al. Genome-wide analysis uncovers novel recurrent alterations in primary central nervous system lymphomas. *Clin Cancer Res*. 2015;21(17):3986-3994. doi:10.1158/1078-0432.CCR-14-2116
- Lim DH, Kim WS, Kim SJ, Yoo HY, Ko YH. Microarray gene-expression profiling analysis comparing PCNSL and non-CNS diffuse large B-cell lymphoma. *Anticancer Res*. 2015;35(6):3333-3340.
- Montesinos-Rongen M, Brunn A, Bentink S, et al. Gene expression profiling suggests primary central nervous system lymphomas to be derived from a late germinal center B cell. *Leukemia*. 2008;22(2):400-405. doi:10.1038/sj.leu.2405019
- Nakamura T, Tateishi K, Niwa T, et al. Recurrent mutations of CD79B and MYD88 are the hallmark of primary central nervous system lymphomas. *Neuropathol Appl Neurobiol*. 2016;42(3):279-290. doi:10.1111/nan.12259
- Fraser E, Gruenberg K, Rubenstein JL. New approaches in primary central nervous system lymphoma. *Chin Clin Oncol*. 2015;4:11.
- Rubenstein JL, Wong VS, Kadoch C, et al. CXCL13 plus interleukin 10 is highly specific for the diagnosis of CNS lymphoma. *Blood*. 2013;121(23):4740-4748. doi:10.1182/blood-2013-01-476333
- Smith JR, Brazier RM, Paoletti S, Lipp M, Uguccioni M, Rosenbaum JT. Expression of B-cell-attracting chemokine 1 (CXCL13) by malignant lymphocytes and vascular endothelium in primary central nervous system lymphoma. *Blood*. 2003;101(3):815-821. doi:10.1182/blood-2002-05-1576
- Brunn A, Montesinos-Rongen M, Strack A, et al. Expression pattern and cellular sources of chemokines in primary central nervous system lymphoma. *Acta Neuropathol*. 2007;114(3):271-276. doi:10.1007/s00401-007-0258-x
- Tateishi K, Miyake Y, Kawazu M, et al. A hyperactive RelA/p65-hexokinase 2 signaling axis drives primary central nervous system lymphoma. *Cancer Res*. 2020;80(23):5330-5343. doi:10.1158/0008-5472.CAN-20-2425
- Pouzoulet F, Alentorn A, Royer-Perron L, et al. Primary CNS lymphoma patient-derived orthotopic xenograft model capture the biological and molecular characteristics of the disease. *Blood Cells Mol Dis*. 2019;75:1-10. doi:10.1016/j.bcmd.2018.11.005
- Jung J, Seol HS, Chang S. The generation and application of patient-derived xenograft model for cancer research. *Cancer Res Treat*. 2018;50(1):1-10. doi:10.4143/crt.2017.307
- Agorku DJ, Tomiuk S, Klingner K, et al. Depletion of mouse cells from human tumor xenografts significantly improves downstream analysis of target cells. *J Vis Exp*. 2016;(113):e54259. doi:10.3791/54259-v

33. Jawhar M, Dohner K, Kreil S, et al. KIT D816 mutated/CBF-negative acute myeloid leukemia: a poor-risk subtype associated with systemic mastocytosis. *Leukemia*. 2019;33(5):1124-1134. doi:[10.1038/s41375-018-0346-z](https://doi.org/10.1038/s41375-018-0346-z)
34. Bolger AM, Lohse M, Usadel B. Trimmomatic: a flexible trimmer for Illumina sequence data. *Bioinformatics*. 2014;30(15):2114-2120. doi:[10.1093/bioinformatics/btu170](https://doi.org/10.1093/bioinformatics/btu170)
35. Dobin A, Davis CA, Schlesinger F, et al. STAR: ultrafast universal RNA-seq aligner. *Bioinformatics*. 2013;29(1):15-21. doi:[10.1093/bioinformatics/bts635](https://doi.org/10.1093/bioinformatics/bts635)
36. Robinson MD, McCarthy DJ, Smyth GK. edgeR: a Bioconductor package for differential expression analysis of digital gene expression data. *Bioinformatics*. 2010;26(1):139-140. doi:[10.1093/bioinformatics/btp616](https://doi.org/10.1093/bioinformatics/btp616)
37. Leek JT, Johnson WE, Parker HS, Jaffe AE, Storey JD. The sva package for removing batch effects and other unwanted variation in high-throughput experiments. *Bioinformatics*. 2012;28(6):882-883. doi:[10.1093/bioinformatics/bts034](https://doi.org/10.1093/bioinformatics/bts034)
38. Wu T, Hu E, Xu S, et al. clusterProfiler 4.0: a universal enrichment tool for interpreting omics data. *Innovation (Camb)*. 2021; 2:100141.
39. Subramanian A, Tamayo P, Mootha VK, et al. Gene set enrichment analysis: a knowledge-based approach for interpreting genome-wide expression profiles. *Proc Natl Acad Sci U S A*. 2005;102(43):15545-15550. doi:[10.1073/pnas.0506580102](https://doi.org/10.1073/pnas.0506580102)
40. Yin Z, Maswikiti EP, Liu Q, et al. Current research developments of patient-derived tumour xenograft models (review). *Exp Ther Med*. 2021;22(5):1206. doi:[10.3892/etm.2021.10640](https://doi.org/10.3892/etm.2021.10640)
41. Herman SE, Sun X, McAuley EM, et al. Modeling tumor-host interactions of chronic lymphocytic leukemia in xenografted mice to study tumor biology and evaluate targeted therapy. *Leukemia*. 2013;27(12):2311-2321. doi:[10.1038/leu.2013.131](https://doi.org/10.1038/leu.2013.131)
42. Hans CP, Weisenburger DD, Greiner TC, et al. Confirmation of the molecular classification of diffuse large B-cell lymphoma by immunohistochemistry using a tissue microarray. *Blood*. 2004;103(1):275-282. doi:[10.1182/blood-2003-05-1545](https://doi.org/10.1182/blood-2003-05-1545)
43. Aronow ME, Shen D, Hochman J, Chan CC. Intraocular lymphoma models. *Ocul Oncol Pathol*. 2015;1(3):214-222. doi:[10.1159/000370158](https://doi.org/10.1159/000370158)
44. Ben Abdelwahed Bagga R, Donnou S, Cosette J, Sautes-Fridman C, Aouni M, Fisson S. Mouse models of primary central nervous system lymphomas: tools for basing funding and therapeutic strategies. *J Neurooncol*. 2015;121(1):9-18. doi:[10.1007/s11060-014-1624-x](https://doi.org/10.1007/s11060-014-1624-x)
45. Babst N, Isbell LK, Rommel F, et al. CXCR4, CXCR5 and CD44 may be involved in homing of lymphoma cells into the eye in a patient derived xenograft homing mouse model for primary vitreoretinal lymphoma. *Int J Mol Sci*. 2022;23(19):11757. doi:[10.3390/ijms231911757](https://doi.org/10.3390/ijms231911757)
46. Nayyar N, White MD, Gill CM, et al. MYD88 L265P mutation and CDKN2A loss are early mutational events in primary central nervous system diffuse large B-cell lymphomas. *Blood Adv*. 2019;3(3):375-383. doi:[10.1182/bloodadvances.2018027672](https://doi.org/10.1182/bloodadvances.2018027672)
47. Montesinos-Rongen M, Godlewska E, Brunn A, Wiestler OD, Siebert R, Deckert M. Activating L265P mutations of the MYD88 gene are common in primary central nervous system lymphoma. *Acta Neuropathol*. 2011;122(6):791-792. doi:[10.1007/s00401-011-0891-2](https://doi.org/10.1007/s00401-011-0891-2)
48. Montesinos-Rongen M, Zuhlke-Jenisch R, Gesk S, et al. Interphase cytogenetic analysis of lymphoma-associated chromosomal breakpoints in primary diffuse large B-cell lymphomas of the central nervous system. *J Neuropathol Exp Neurol*. 2002;61(10):926-933. doi:[10.1093/jnen/61.10.926](https://doi.org/10.1093/jnen/61.10.926)
49. Dave BJ, Weisenburger DD, Higgins CM, et al. Cytogenetics and fluorescence in situ hybridization studies of diffuse large B-cell lymphoma in children and young adults. *Cancer Genet Cytogenet*. 2004;153(2):115-121. doi:[10.1016/j.cancergencyto.2004.01.008](https://doi.org/10.1016/j.cancergencyto.2004.01.008)
50. Yamada K, Kasama M, Kondo T, Shinoura N, Yoshioka M. Chromosome studies in 70 brain tumors with special attention to sex chromosome loss and single autosomal trisomy. *Cancer Genet Cytogenet*. 1994;73(1):46-52. doi:[10.1016/0165-4608\(94\)90180-5](https://doi.org/10.1016/0165-4608(94)90180-5)
51. Russell LM, Strike P, Browne CE, Jacobs PA. X chromosome loss and ageing. *Cytogenet Genome Res*. 2007;116(3):181-185. doi:[10.1159/000098184](https://doi.org/10.1159/000098184)
52. Montesinos-Rongen M, Schafer E, Siebert R, Deckert M. Genes regulating the B cell receptor pathway are recurrently mutated in primary central nervous system lymphoma. *Acta Neuropathol*. 2012;124(6):905-906. doi:[10.1007/s00401-012-1064-7](https://doi.org/10.1007/s00401-012-1064-7)
53. Phelan JD, Young RM, Webster DE, et al. A multiprotein supercomplex controlling oncogenic signalling in lymphoma. *Nature*. 2018; 560(7718):387-391. doi:[10.1038/s41586-018-0290-0](https://doi.org/10.1038/s41586-018-0290-0)
54. Cordone I, Masi S, Carosi M, et al. Brain stereotactic biopsy flow cytometry for central nervous system lymphoma characterization: advantages and pitfalls. *J Exp Clin Cancer Res*. 2016;35(1):128. doi:[10.1186/s13046-016-0404-1](https://doi.org/10.1186/s13046-016-0404-1)
55. Deblquis A, Voirin J, Harzallah I, et al. Cytomorphology and flow cytometry of brain biopsy rinse fluid enables faster and multidisciplinary diagnosis of large B-cell lymphoma of the central nervous system. *Cytometry B Clin Cytom*. 2018;94(1):182-188. doi:[10.1002/cyto.b.21403](https://doi.org/10.1002/cyto.b.21403)
56. Bashir R, Coakham H, Hochberg F. Expression of LFA-1/ICAM-1 in CNS lymphomas: possible mechanism for lymphoma homing into the brain. *J Neurooncol*. 1992;12(2):103-110. doi:[10.1007/BF00172658](https://doi.org/10.1007/BF00172658)
57. Deckert M, Montesinos-Rongen M, Brunn A, Siebert R. Systems biology of primary CNS lymphoma: from genetic aberrations to modeling in mice. *Acta Neuropathol*. 2014;127(2):175-188. doi:[10.1007/s00401-013-1202-x](https://doi.org/10.1007/s00401-013-1202-x)
58. Tun HW, Personett D, Baskerville KA, et al. Pathway analysis of primary central nervous system lymphoma. *Blood*. 2008;111(6):3200-3210. doi:[10.1182/blood-2007-10-119099](https://doi.org/10.1182/blood-2007-10-119099)
59. Jiang L, Marlow LA, Cooper SJ, et al. Selective central nervous system tropism of primary central nervous system lymphoma. *Int J Clin Exp Pathol*. 2010;3(8):763-767.
60. He M, Zhang W, Wang J, et al. Aggregative perivascular tumor cell growth pattern of primary central nervous system lymphomas is associated with hypoxia-related endoplasmic reticulum stress. *J Cancer*. 2021;12(13):3841-3852. doi:[10.7150/jca.54952](https://doi.org/10.7150/jca.54952)
61. Jankauskas SS, Wong DWL, Bucala R, Djudjaj S, Boor P. Evolving complexity of MIF signaling. *Cell Signal*. 2019;57:76-88. doi:[10.1016/j.cellsig.2019.01.006](https://doi.org/10.1016/j.cellsig.2019.01.006)
62. Ntanasis-Stathopoulos I, Fotiou D, Terpos E. CCL3 signaling in the tumor microenvironment. *Adv Exp Med Biol*. 2020;1231:13-21. doi:[10.1007/978-3-030-36667-4_2](https://doi.org/10.1007/978-3-030-36667-4_2)
63. Baba T, Mukaida N. Role of macrophage inflammatory protein (MIP)-1alpha/CCL3 in leukemogenesis. *Mol Cell Oncol*. 2014;1(1):e29899. doi:[10.4161/mco.29899](https://doi.org/10.4161/mco.29899)
64. Abe M, Hiura K, Wilde J, et al. Role for macrophage inflammatory protein (MIP)-1alpha and MIP-1beta in the development of osteolytic lesions in multiple myeloma. *Blood*. 2002;100(6):2195-2202. doi:[10.1182/blood.V100.6.2195](https://doi.org/10.1182/blood.V100.6.2195)
65. Montesinos-Rongen M, Siebert R, Deckert M. Primary lymphoma of the central nervous system: just DLBCL or not? *Blood*. 2009;113(1):7-10. doi:[10.1182/blood-2008-04-149005](https://doi.org/10.1182/blood-2008-04-149005)
66. Zhang J, Zhu Z, Miao Z, et al. The clinical significance and mechanisms of REG4 in human cancers. *Front Oncol*. 2020;10:559230. doi:[10.3389/fonc.2020.559230](https://doi.org/10.3389/fonc.2020.559230)
67. Sninsky JA, Bishnupuri KS, Gonzalez I, Trikalinos NA, Chen L, Dieckgraefe BK. Reg4 and its downstream transcriptional activator CD44ICD in stage II and III colorectal cancer. *Oncotarget*. 2021; 12(4):278-291. doi:[10.18632/oncotarget.27896](https://doi.org/10.18632/oncotarget.27896)

68. Yuan J, Gu K, He J, Sharma S. Preferential up-regulation of osteopontin in primary central nervous system lymphoma does not correlate with putative receptor CD44v6 or CD44H expression. *Hum Pathol.* 2013;44(4):606-611. doi:[10.1016/j.humpath.2012.07.007](https://doi.org/10.1016/j.humpath.2012.07.007)

SUPPORTING INFORMATION

Additional supporting information can be found online in the Supporting Information section at the end of this article.

How to cite this article: Isbell LK, Tschuch C, Doostkam S, et al. Patient-derived xenograft mouse models to investigate tropism to the central nervous system and retina of primary and secondary central nervous system lymphoma. *Neuropathol Appl Neurobiol.* 2023;49(2):e12899. doi:[10.1111/nan.12899](https://doi.org/10.1111/nan.12899)